



Copyright Notice

©2012 IEEE. Personal use of this material is permitted. However, permission to reprint/republish this material for advertising or promotional purposes or for creating new collective works for resale or redistribution to servers or lists, or to reuse any copyrighted component of this work in other works must be obtained from the IEEE.

This document was downloaded from Chalmers Publication Library (<http://publications.lib.chalmers.se/>), where it is available in accordance with the IEEE PSPB Operations Manual, amended 19 Nov. 2010, Sec. 8.1.9 (<http://www.ieee.org/documents/opsmanual.pdf>)

(Article begins on next page)

A Discrete-Time Model for Uncompensated Single-Channel Fiber-Optical Links

Lotfollah Beygi, Erik Agrell, Pontus Johannisson, Magnus Karlsson, and Henk Wymeersch

Abstract—An analytical discrete-time model is introduced for single-wavelength polarization multiplexed nonlinear fiber-optical channels based on the symmetrized split-step Fourier method (SSFM). According to this model, for high enough symbol rates, a fiber-optic link can be described as a linear dispersive channel with additive white Gaussian noise (AWGN) and a complex scaling. The variance of this AWGN noise and the attenuation are computed analytically as a function of input power and channel parameters. The results illustrate a cubic growth of the noise variance with input power. Moreover, the cross effect between the two polarizations and the interaction of amplifier noise and the transmitted signal due to the nonlinear Kerr effect are described. In particular, it is found that the channel noise variance in one polarization is affected twice as much by the transmitted power in that polarization than by the transmitted power in the orthogonal polarization. The effect of pulse shaping is also investigated through numerical simulations. Finally, it is shown that the analytical performance results based on the new model are in close agreement with numerical results obtained using the SSFM for a symbol rate of 28 Gbaud and above.

Index Terms—Channel modeling, Nonlinear fiber-optic channels, Chromatic dispersion, Nonlinear phase-noise, Symmetrized split-step Fourier method (SSFM), Nonlinear Schrödinger equation (NLSE).

I. INTRODUCTION

THE growing demand for high data rates in optical networks encourages applying advanced coding and modulation techniques in fiber-optical channels [1], [2], which exploit the available bandwidth more efficiently. The design of advanced coded modulation techniques requires an accurate channel model [3], [4]. Moreover, the Shannon channel coding theorem, which is used as a criterion in the design of coded modulation schemes, also requires an exact channel model and signal statistics [5]–[7].

The propagation of light in optical fibers is described by the nonlinear Schrödinger equation (NLSE). These channels are nonlinear with non-Gaussian noise, and due to the lack of analytical solutions and the complexity of numerical approaches, deriving the statistics of such channels is in general cumbersome. Hence, many efforts have been devoted to computing the statistics for simplified models, e.g., memory-less nonlinear channels with single- [8], [9, p. 225] and dual-polarization (DP) [10] signals, partially coherent linear channels [11]–[13], and a channel with intra-channel four-wave mixing (IFWM) [14], [15].

The authors are with Chalmers University of Technology, Sweden (email: beygil, agrell, pontus.johannisson, magnus.karlsson, and henkw@chalmers.se). The research supported by the Swedish Foundation for Strategic Research, SSF, under grant RE07-0026 and by VINNOVA under grant 2010-01238.

Considering linear and nonlinear effects, an analytical expression for the variance of nonlinear phase noise [16] was introduced in [17]. This result was based on a first-order perturbation technique. Ho and Wang [18] analyzed the variance of the nonlinear phase noise by including the effect of intrachannel cross-phase modulation and chromatic dispersion (CD). A model based on a combined regular-logarithmic perturbation method [19] was proposed for the simultaneous presence of nonlinear and dispersive effects. Moreover, an approximate expression for the probability density function (pdf) of the phase difference of an optical and electrical filtered signal has been proposed in [20]. The time domain, frequency domain, and Fourier series method based on the saddle point approximation were compared in [21] for intensity- and phase-modulated direct-detection optically amplified systems. A discrete-time model based on a Volterra series transfer function method was proposed in [22], which is suitable for time-division multiplexed transmission at high symbol rate.

Although the above-mentioned approaches clarified many aspects of a fiber-optical channel, an accurate statistical channel model with known pdf of the received signal was lacking for a channel without inline CD compensation. However, according to [23], an optical fiber channel with electronic dispersion compensation (EDC) at the receiver and without inline CD compensation, which is operating at high symbol rates, can be modeled as an additive white Gaussian noise (AWGN) channel. Later, an analytical model was proposed for a fiber-optic link using wavelength-division multiplexing (WDM) [24]–[26]. The power spectral density of nonlinear noise was given by a closed-form formula and the theoretical results were in close agreement with the numerical simulations. Bononi et al. [27] derived a nonlinear interference coefficient for the IFWM-dominant regime and showed that their result is consistent with [25] for the cross-phase modulation (XPM) dominant regime.

The aim of this paper is to derive an analytical channel model for a polarization-multiplexed single-channel fiber-optic link without inline CD compensation. We show analytically that for high symbol rates (as illustrated in Fig. 1(c)), the fiber-optic link depicted in Fig. 1(a) can be modeled as a linear AWGN channel with a complex multiplication as shown in Fig. 1(b). In the analysis, we take into account the cross effect of the signals in both polarizations. In contrast to previous works [25], [26], [28], we include the inline interaction between the transmitted signal and the amplified spontaneous emission (ASE) noise in different spans due to the Kerr effect. Moreover, a closed-form expression for the variance of the AWGN noise and the channel attenuation are

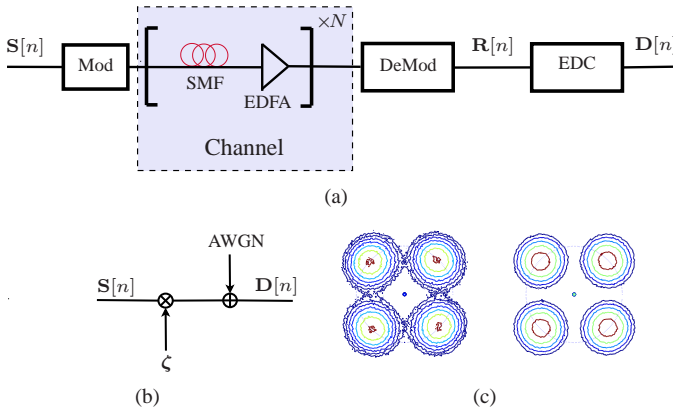


Fig. 1. (a) A fiber-optical link with N spans. Each span consists of an SMF and an EDFA (the modulator (Mod) converts the discrete-time signal from the signal space to a continuous-time optical signal and the demodulator (DeMod) converts the received optical signal to a baseband discrete-time signal). (b) The introduced discrete-time equivalent model (ζ is a complex vector). (c) The contours of the two-dimensional histograms for the received QPSK signal simulated by the SSFM for the symbol rate 14 Gbaud on the left side and 28 Gbaud on the right side.

derived as a function of the transmitted power and the channel parameters. It is also shown that the channel noise variance in one polarization is affected twice as much by the transmitted power in that polarization than by the transmitted power in the orthogonal polarization. This fact has been previously reported in [26] and implicitly in [29], [30]. The power loss in the fiber-optic link is compensated by inline amplifiers, and therefore the above mentioned attenuation is coming from the fact that the nonlinear effect converts a part of the transmitted power to noise-like interference [13].

The symbol error rate (SER) of a DP quadrature phase shift keying (DP-QPSK) system is computed both analytically and using the split-step Fourier method (SSFM). The performance comparison shows a close agreement between the results. Finally, it is shown both analytically and numerically that the system performance will be improved by increasing the CD.

Notation: We use $x[n] \triangleq x(nT)$ to denote the samples of any signal $x(t)$ at $t = nT$. All continuous- and discrete-time random variables and random processes are shown with capital letters. DP signals are denoted by a boldface vector. $\angle x$ denotes the angle of the complex variable x . The real and imaginary parts of a complex variable x are denoted by $\text{Re}(x)$ and $\text{Im}(x)$, respectively. $[x]$ represents the greatest integer less than or equal to x . The squared Euclidean norm of a complex vector \mathbf{x} is denoted by $\|\mathbf{x}\|^2$ and $\mathbb{E}\{\cdot\}$ denotes expectation. Finally, all deterministic signals have lowercase letters, as have outcomes (realizations) of random processes and variables.

II. CONTINUOUS-TIME MODEL

The NLSE describes the light propagation in an optical fiber as [31, ch. 6]

$$j \frac{\partial \mathbf{u}(t, z)}{\partial z} - \frac{\beta_2}{2} \frac{\partial^2 \mathbf{u}(t, z)}{\partial t^2} + \gamma (\mathbf{u}(t, z) \mathbf{u}(t, z)^\dagger) \mathbf{u}(t, z) + j \frac{\alpha}{2} \mathbf{u}(t, z) = \mathbf{0}, \quad (1)$$

where \mathbf{u} is the DP electric field with complex components (u_x, u_y) , γ is the fiber nonlinear coefficient, α is the attenua-

tion coefficient, β_2 is the group velocity dispersion, \dagger denotes Hermitian conjugation, t is the time coordinate in a co-moving reference frame and z is the propagation distance. Here, we used equations (6.1.22) and (6.1.23) of [31] with $B = 1$ based on the Manakov model [32] and $\beta_{1x} = \beta_{1y} = 0$, which is an approximation obtained by averaging over fast polarization rotations in the Manakov equation. This equation automatically prevents taking into account polarization mode dispersion (PMD) effects and therefore restricts the analysis to the (practically relevant) case of low-PMD fibers. A fiber-optical link with N spans of length L is considered according to Fig. 1(a). Each span consists of a standard single-mode fiber (SMF) followed by an erbium-doped fiber amplifier (EDFA).

In this paper, we use the SSFM [31, eq. 2.4.10] both to construct the analytical discrete-time model as well as to simulate a fiber-optic channel numerically. In fact, the SSFM provides an appropriate mathematical model which can be used to derive the signal statistics by following an analytical approach. In this method, each SMF span is modeled by a concatenation of M segments with linear and nonlinear effects as shown in Fig. 2. The length of each segment, L/M , should be chosen small enough to ensure that the linear and nonlinear effects act independently. The linear propagation can be described in the time domain [33], [34] as a solution of (1) for $\gamma = 0$ by $\mathbf{u}(t, z) = e^{-\alpha z/2} \mathbf{u}(t, 0) * h(t, z)$, where $*$ denotes convolution and $h(t, z) = e^{j(t^2/(2\beta_2 z))} / \sqrt{j2\pi\beta_2 z}$ is the dispersive impulse response¹. As shown in Fig. 2, the linear effect in each segment is considered in two steps, the linear propagation in the first (linear) stage of each segment is described by $\mathbf{u}(t, (m-1/2)L/M) = e^{-\alpha L/(4M)} \mathbf{u}(t, (m-1)L/M) * h(t, L/(2M))$, $m = 1, \dots, M$. The nonlinear effect of each segment, described by the solution of (1) for $\beta_2 = 0$, is given by

$$\tilde{\mathbf{u}}(t, (m-1/2)\frac{L}{M}) = \mathbf{u}(t, (m-1/2)\frac{L}{M}) e^{j\mu \|\mathbf{u}(t, (m-1/2)\frac{L}{M})\|^2}, \quad (2)$$

where $m = 1, \dots, M$ and $\mu = 2\gamma\alpha^{-1} \sinh(\alpha L/(2M))$ [31, sec 4.1.1]². Finally, CD and attenuation operate on the output of the nonlinear unit in the second stage of the segment as $\mathbf{u}(t, mL/M) = e^{-\alpha L/4M} \tilde{\mathbf{u}}(t, (m-1/2)L/M) * h(t, L/(2M))$, $m = 1, \dots, M$. The symbols $\mathbf{S}[n] = (S_x[n], S_y[n])$, e.g., DP-QPSK, are transmitted every T seconds with a pulse shaping filter $g(t)$. It is assumed that $\mathbb{E}\{|S_x[n]|^2\} = P_x T$, where P_x is the transmitted power in polarization x . The statistics of the received signal are derived for a given transmitted symbol $S_x[0] = s_x$ at time instant $t = 0$.

We assume that each EDFA compensates for the attenuation in each fiber span and adds a circular white complex Gaussian ASE noise vector, $\mathbf{Z}_i(t) = (Z_x^i(t), Z_y^i(t))$ in each span with variance $\sigma^2 = GF_n h\nu_{\text{opt}}/(2T)$ in each polarization [35, eq. 8.1.15], where G is the required gain to compensate for the attenuation in a span, $F_n = 2n_{\text{sp}}(1 - G^{-1})$ is the noise

¹The CD filter has the all-pass frequency response $H(f, z) = e^{-j2\pi^2\beta_2 z f^2}$ [34].

²In contrast to [31, sec 4.1.1], the nonlinear phase noise is written as a function of the signal at the mid-point of the segment and a factor $e^{\alpha L/(2M)}$ compensates for the signal attenuation at this point.

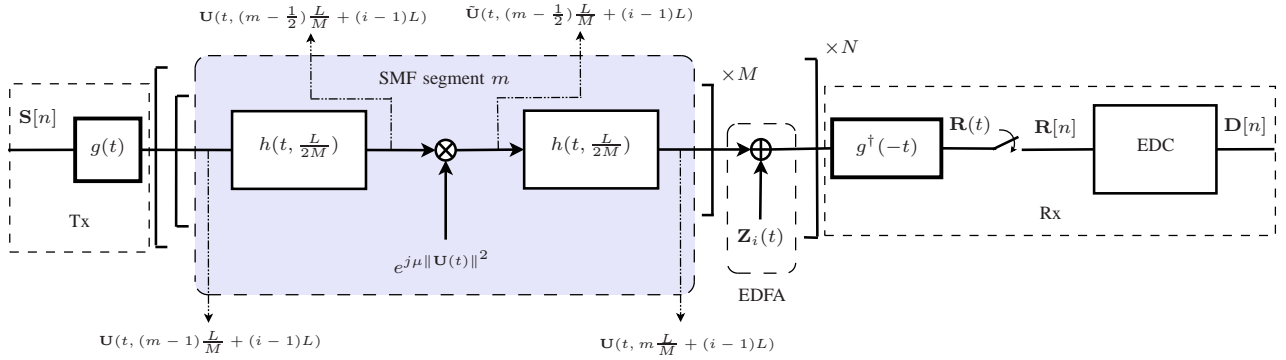


Fig. 2. A baseband continuous-time model for a fiber-optical link with N spans $i = 1, \dots, N$, each consists of M segments $m = 1, \dots, M$, and electronic chromatic post compensation (for simplicity, fiber attenuations and amplifier gains have been dropped).

figure, in which n_{sp} is ASE noise factor, and $h\nu_{\text{opt}}$ is the photon energy. The linear SNR in polarization x is denoted by $\rho_x \triangleq P_x/(N\sigma^2)$. We also define $\eta \triangleq L/(ML_D)$, in which $L_D = T^2/|\beta_2|$ is the dispersion length [31, p. 55]. The optical bandwidth of the EDFAs is assumed to be equal to the signal bandwidth. The dispersion is compensated for by electronic dispersion compensation (EDC). This EDC filter, $h(t, -NL)$, is the N -fold convolution of the inverse of the CD filter of each span with itself. In order to apply an analytical approach, we consider sinc-shaped pulses. However, the numerical results show the accuracy of the proposed model for other pulse shapes, e.g., raised cosine and Gaussian pulses. A matched filter to the pulse shape with a Nyquist sampler is assumed at the receiver.³ Due to the symmetry, we perform the derivations only for one polarization, denoted x , except where otherwise stated.

III. DISCRETE-TIME MODEL

In this section, the continuous-time SSFM is used to derive a discrete-time model. To find the distribution of the received signal for a transmitted symbol, we assume the complex symbol $\mathbf{s} = (s_x, s_y)$ is transmitted at time instant $t = 0$ and symbols before and after this time instant are unknown to the detector, i.e., no nonlinear pre- or post-compensation technique such as digital backpropagation [36] is used. First, we describe the signal propagation for segment m from span i shown in Fig. 3(a) from the fiber-optical link described in Fig. 2 and the statistics of the received signal for this segment are derived in Section IV. Then, in Section V, we extend the results for one segment to a fiber-optical link with N spans.

In the continuous-time model considering $g(t) = \text{sinc}(t/T)/\sqrt{T}$ as a pulse shape, where $\text{sinc}(x) = (\sin \pi x)/(\pi x)$, the transmitted signal is band-limited to $[-\frac{1}{2T}, \frac{1}{2T}]$. Hereafter, we assume a quasi-linear fiber-optical data transmission [37], therefore we neglect the spectral broadening due to the nonlinear effects, i.e., the bandwidth of $U_x(t)e^{j\mu \|U(t)\|^2}$ is assumed to be limited to $1/T$. This assumption helps us to obtain the discrete-time model depicted in Fig. 3(a) for segment m from span i , consisting of Stages 1 and 2. In this figure, the band-limited CD filter is given⁴ by

$$h[n] = h\left(t, \frac{L}{2M}\right) * \text{sinc}\left(\frac{t}{T}\right) \Big|_{t=nT}. \quad (3)$$

³Perfect carrier and timing synchronization are assumed.

⁴For a sinc(\cdot) pulse, $g^\dagger(-t) = g(t)$.

The output of Stage 1 in Fig. 3(a) for input $\mathbf{V}_{i,m-1}[n] = (V_{x_{m-1}^i}[n], V_{y_{m-1}^i}[n])$, is

$$\mathbf{U}_{i,m}[n] = A \sum_{k=-\infty}^{\infty} \mathbf{V}_{i,m-1}[n-k]h[k], \quad (4)$$

where $\mathbf{U}_{i,m}[n] = (U_{x_m^i}[n], U_{y_m^i}[n])$ and $A = e^{-\frac{\alpha}{4}\eta L_D}$. According to the discrete-time model given in Fig. 3(a), the output signal of Stage 2, $\mathbf{V}_{i,m}[n]$, can be decomposed into a linear term $\mathbf{V}_{L_m^i}[n] = (V_{Lx_m^i}[n], V_{Ly_m^i}[n])$ and a nonlinear term $\mathbf{V}_{NL_m^i}[n] = (V_{NLx_m^i}[n], V_{NLY_m^i}[n])$ as

$$\mathbf{V}_{i,m}[n] = \mathbf{V}_{L_m^i}[n] + \mathbf{V}_{NL_m^i}[n], \quad (5)$$

where

$$V_{Lx_m^i}[n] = A\zeta_{x_m^i}[n]U_{x_m^i}[n] * h[n], \quad (6)$$

$$V_{NLx_m^i}[n] = AB_{x_m^i}[n] * h[n], \quad (7)$$

in which $B_{x_m^i}[n] = U_{x_m^i}[n] \left(e^{j\mu \|U_{i,m}[n]\|^2} - \zeta_{x_m^i}[n] \right)$. The term $V_{NLx_m^i}$ will be referred to as *nonlinear noise* [24]. In a similar way, equations (6)–(7) can be written for polarization y . Clearly, (5)–(7) hold for any complex vector $\zeta_{i,m} = (\zeta_{x_m^i}, \zeta_{y_m^i})$, however we will choose this complex vector such that the mean of $V_{NLx_m^i}$ and $V_{NLY_m^i}$ is zero. An equivalent linear discrete-time model for Stage 2 of Fig. 3(a) is shown in Fig. 3(b) exploiting (5)–(7).

IV. STATISTICS OF THE PROPAGATED SIGNAL

We proceed with the derivation of the statistics of segment m shown in Fig. 3(a), for an asymptotic case of strong dispersive effects, i.e., $\eta \rightarrow \infty$. Although this scenario is not exactly valid for a real system, it helps us to get some insight into the qualitative channel behavior in a real fiber-optical link.

A. Signal statistics for the case of strong dispersive effects

For a given transmitted symbol $S_x[0] = s_x$ and $\eta \rightarrow \infty$, we investigate the signal statistics of the single-segment scheme shown in Fig. 3(a).

Lemma 1: In segment m of span i shown in Fig. 3(a), the samples $U_{x_m^i}[n]$ are a sequence of complex independent Gaussian random variables.

Proof: See Appendix A. ■

The mean of the nonlinear noise is given by $\mathbb{E}\{V_{NLx_m^i}[n]|S_x[0]\} = A\mathbb{E}\{B_{x_m^i}[n]|S_x[0]\} * h[n]$. Using

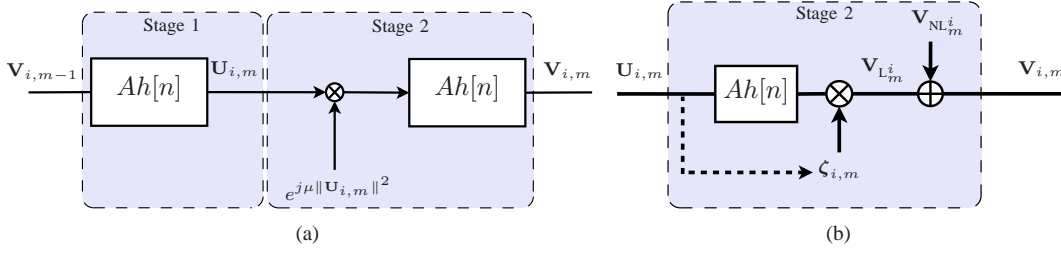


Fig. 3. (a) An equivalent discrete-time channel model of segment m from span i of the fiber-optical link given in Fig. 2. (b) The equivalent linear model of Stage 2 in Fig. 3(a) with an additive nonlinear noise $\mathbf{V}_{NL_m^i}[n]$ and a complex scaling $\zeta_{i,m}$, which depends on $\mathbf{U}_{i,m}$. The filter attenuation is $A = e^{-\frac{\alpha}{4}\eta L_D}$.

Proposition 1 in Appendix B, we get

$$\mathbb{E} \left\{ B_{x_m^i}[n] \middle| S_x[0] \right\} = \bar{U}_{x_m^i}[n] \left[\Phi_{x_m^i}^2[n] \Phi_{y_m^i}[n] \right. \\ \left. \times e^{j\mu (\Phi_{x_m^i}[n] |\bar{U}_{x_m^i}[n]|^2 + \Phi_{y_m^i}[n] |\bar{U}_{y_m^i}[n]|^2)} - \zeta_{x_m^i}[n] \right],$$

where $\bar{U}_{x_m^i}[n] = \mathbb{E}\{U_{x_m^i}[n] | S_x[0]\}$,

$$\begin{aligned} \Phi_{x_m^i}^{-1}[n] &= 1 - j\mu \text{Var}(U_{x_m^i}[n]), \\ \Phi_{y_m^i}^{-1}[n] &= 1 - j\mu \text{Var}(U_{y_m^i}[n]). \end{aligned} \quad (8)$$

Here, we find the channel complex scaling such that the mean of the nonlinear noise is zero. Thus,

$$\zeta_{x_m^i}[n] = \Phi_{x_m^i}^2[n] \Phi_{y_m^i}[n] e^{j\mu (\Phi_{x_m^i}[n] |\bar{U}_{x_m^i}[n]|^2 + \Phi_{y_m^i}[n] |\bar{U}_{y_m^i}[n]|^2)}. \quad (9)$$

Lemma 2: The nonlinear noise, $V_{NLx_m^i}$ and $V_{NLY_m^i}$, are independent zero-mean proper⁵ [38] complex AWGNs. Moreover, the linear terms $V_{Lx_m^i}$ and $V_{Ly_m^i}$ are independent of the nonlinear noises $V_{NLx_m^i}$ and $V_{NLY_m^i}$.

Proof: See Appendix C. ■

B. Signal statistics for a segment length applicable to SSFM

In this section, we investigate the results for finite values of η . Although the convergence to a Gaussian distribution in Lemma 1 is proven for an asymptotic case with a $\text{sinc}(\cdot)$ pulse shape, the signal distribution can be approximated very well by a Gaussian distribution for a fiber-optical link also with a root raised cosine (RRC) pulse shape or a Gaussian pulse shape.

We note a subtle point in the selection of the segment length. In contrast to the numerical SSFM, the segment length cannot be chosen arbitrarily small. Each output sample of the CD filter is written as a sum of input symbols weighted by CD filter coefficients. Since the minimum required independent sample size to sum to a Gaussian distribution varies for different input pdfs, the generalized criterion may not be applicable. By an empirical approach, we found that $L/M > 0.5L_D$ is necessary to get a Gaussian distribution at the output of the CD filter. On the other hand, it is observed that $L/M < L_D$ gives enough accuracy for the numerical solution of the NLSE based on the SSFM. Therefore, in the rest of the analysis, we set $0.5 < \eta < 1$ and

⁵A complex random variable Z is proper if its pseudo-covariance, $\mathbb{E}\{(Z - \bar{Z})^2\}$, is zero or equivalently its real and imaginary part are uncorrelated and have the same variance of $\mathbb{E}\{|Z - \bar{Z}|^2\}/2$.

$$\frac{L}{M} = \eta L_D. \quad (10)$$

In contrast, for the numerical SSFM, it is better to use a very small segment size.

1) *The channel complex scaling and the nonlinear noise variance of a segment:* In order to apply an analytical approach, we assume that the results of Lemmas 1 and 2 hold for a finite segment length, i.e., $L/M = \eta L_D$. Our approach to derive the signal statistics of segment m is based on the discrete-time model given in Fig. 3(a) and it can be simply described as follows: First, one may use Lemma 1 to conclude that the signal at the output of *Stage 1* is a Gaussian random process. Then, we replace *Stage 2* with a linear model shown in Fig. 3(b). According to this transform, the nonlinear effect has the same effect as converting a part of the signal to noise-like interference or nonlinear noise. Exploiting Lemma 2, it is seen that the nonlinear noise, $\mathbf{V}_{NL_m^i}$, is AWGN. Moreover, we note that using Lemma 2, one can conclude that the components of this nonlinear noise in the two polarizations are independent and the nonlinear noise is independent of the signal term. Finally, the concatenation of Stages 1 and 2 is modeled by a linear channel with an AWGN and the CD filter $h[n] * h[n]$.

Here, we introduce $\phi_x \triangleq \gamma \alpha^{-1} P_x$; $\phi_x \ll 1$. Then, as shown in Appendix D, the channel attenuation and the nonlinear noise variance of segment m from span i can be approximated by

$$|\zeta_{x_m^i}|^2 \approx 1 - 4 \sinh^2\left(\frac{\alpha}{2}\eta L_D\right) \left[2 + \kappa^2 + 2(i-1) \frac{2+\kappa}{N\rho_x} \right. \\ \left. + (i-1)^2 \frac{3}{N^2\rho_x^2} \right] \phi_x^2 A^{8m-4}, \quad (11)$$

$$\sigma_{NLx_m^i}^2 \approx (1 - |\zeta_{x_m^i}|^2) A^{4m} P_x, \quad (12)$$

where $\kappa = P_y/P_x$ and $\sigma_{NLx_m^i}^2$ is the variance of the nonlinear noise for segment m from span i in polarization x . We note that the channel attenuation of each segment, (11), is affected by the signal and the ASE noise. We also note that since the channel is nonlinear, the signal and the ASE noise cannot be treated independently.

One may compute the pdf of the signal at the output of stage 1 (see Fig. 3(a)) for Segments 1 and 4 using numerical SSFM. As seen in Fig. 4, the pdf of the electric signal at the output of stage 1 can be approximated very well by a Gaussian pdf for segments 4 and onward. This fact has been used in Appendix D to motivate the exploited approximation in the derivation of equations (11) and (12).

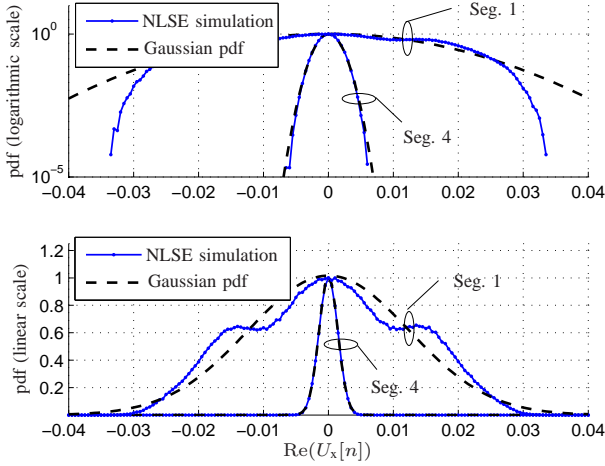


Fig. 4. The pdf of $\text{Re}(U_x[n])$ at the output of stage 1 (see Fig. 3(a)) in segments 1 and 4 of span 1 for System IV introduced in Table I (with a span length of 125 km and a symbol rate of 28 Gbaud). The solid curves are the results of NLSE simulation with SSFM and the dashed curves are the approximated Gaussian distributions.

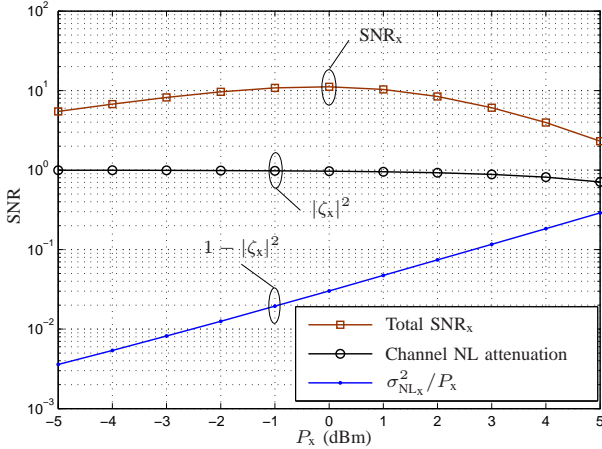


Fig. 5. The total SNR_x ($|\zeta_x|^2 P_x / (N\sigma^2 + \sigma_{\text{NL}_x}^2)$), the channel attenuation due to fiber nonlinearities (Channel NL attenuation), and the normalized variance of nonlinear-noise ($\sigma_{\text{NL}_x}^2 / P_x = 1 - |\zeta_x|^2$) for System IV in Table I with a symbol rate of 28 Gbaud and a dispersion coefficient of $D = 17$ ps/nm/km.

V. STATISTICS OF THE RECEIVED SIGNAL

In this section, we use (11) and (12) to derive a model for a general fiber-optical link. Since the SSFM is accurate for a small segment-length, for a typical span length (50–120 km), one may consider M segments for each span to get enough accuracy. On the other hand, as discussed in Section IV, M must be small enough to obtain a Gaussian distribution at the output of the CD filter. A segment length around ηL_D , $0.5 < \eta < 1$, provides enough CD, i.e., a CD filter with a sufficient number of non-zero coefficients. The results for a segment, (11) and (12), can be extended to a fiber-optical link with N spans, each consisting of an SMF and an EDFA. Consequently, a fiber-optical link with N spans can be modeled by a linear channel with zero-mean AWGN and a complex scaling as shown in Fig. 1(b). Here, the channel complex scaling and the system SNR are derived exploiting (11) and (12).

Theorem 1: Assuming equalities in (11) and (12), the squared amplitude of the channel complex scaling in polarization x , shown in Fig. 1(b), is

$$|\zeta_x|^2 = 1 - N\phi_x^2 \left[2 + \kappa^2 + \left(1 - \frac{1}{N}\right) \frac{2+\kappa}{\rho_x} + \left(2 - \frac{3}{N} + \frac{1}{N^2}\right) \frac{1}{2\rho_x^2} \right] \times \tanh\left(\frac{\alpha}{2}\eta L_D\right) (1 - e^{-2\alpha L}). \quad (13)$$

The system SNR in polarization x is $\text{SNR}_x = |\zeta_x|^2 P_x / (N\sigma^2 + \sigma_{\text{NL}_x}^2)$, where

$$\sigma_{\text{NL}_x}^2 = P_x (1 - |\zeta_x|^2). \quad (14)$$

Proof: See Appendix E. ■

It is clearly seen from (13) and (14) that the contribution of signal-noise interaction to the variance of the nonlinear noise is considerably ($\approx \rho_x$ times for polarization x) smaller than the contribution of the signal-signal interaction. This finding is consistent with [25]–[28], which simulate ASE noise as concentrated at the receiver for uncompensated systems without nonlinear equalization. The results of Theorem 1 can be simplified for $\rho_x \gg 1$ and neglecting the Taylor expansion terms of order higher than ϕ_x^2 , as

$$|\zeta_x|^2 \approx 1 - N\phi_x^2 (2 + \kappa^2) \tanh\left(\frac{\alpha}{2}\eta L_D\right), \\ \sigma_{\text{NL}_x}^2 \approx N\phi_x^2 P_x (2 + \kappa^2) \tanh\left(\frac{\alpha}{2}\eta L_D\right), \quad (15)$$

where we also used $1 - e^{-2\alpha L} \approx 1$. As seen from (15), the total nonlinear noise variance in a fiber-optical channel in one polarization gets twice the effect from the power in the corresponding polarization than the power in the orthogonal polarization. For linear modulation formats, the minimum symbol error rate of polarization x (SER_x) is attained for the maximum achievable SNR_x . One may find this maximum SNR_x by $\partial(\text{SNR}_x)/\partial P_x = 0$, ($\kappa = 1$) and then solving

$$2P_x^3 + 3N\sigma^2 P_x^2 - \frac{\sigma^2}{2 + \kappa^2} \coth\left(\frac{\alpha}{2}\eta L_D\right) = 0. \quad (16)$$

In Fig. 5, the total SNR_x ($|\zeta_x|^2 P_x / (N\sigma^2 + \sigma_{\text{NL}_x}^2)$), the channel attenuation due to fiber nonlinearities ($|\zeta_x|^2$), and the normalized variance of nonlinear-noise ($\sigma_{\text{NL}_x}^2 / P_x = 1 - |\zeta_x|^2$) for System IV in Table I (with a symbol rate of 28 Gbaud and a dispersion coefficient of $D = 17$ ps/nm/km) are plotted versus the transmitted power P_x . This figure illustrates the cubic growth of the nonlinear noise variance with the input power.

VI. NUMERICAL RESULTS

In this section, we evaluate the accuracy of the derived model for four fiber-optical systems with parameters given in Table I. The calculation is performed both analytically and numerically. For the numerical SSFM, the Manakov equation is used to model the nonlinear propagation with two polarizations with segment size of $L_D/10$. In the simulations, the receiver is assumed to have perfect knowledge of the polarization state. Moreover, the ASE noise with a variance of $\sigma^2 = WS$ is added in each span (lumped amplification), where W is the bandwidth of the EDFA filters and $S = GF_n h\nu_{\text{opt}}/2$, in which $F_n = 2n_{\text{sp}}(1 - G^{-1})$ is the noise figure of EDFA amplifier (see Section II). The EDFA filters are assumed to be unity gain with double-sided bandwidth equal to the exploited sampling frequency, which is usually greater than the signal bandwidth.

TABLE I
FOUR SIMULATED SYSTEMS WITH EDC AT THE RECEIVER.

System	I	II	III	IV
$1/T$ (Gbaud)	44	33.3	33.3	28
D (ps/nm/km)	17	24	17	17
n_{sp}	1.7	1.7	1.7	2
η	0.66	0.6	0.6	0.53

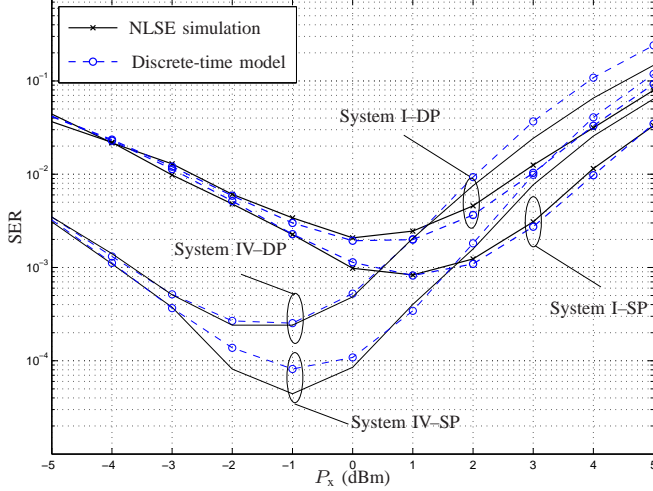


Fig. 6. The SER of Systems I and IV with single-polarization (SP) and dual-polarization (DP)-QPSK versus transmitted power per polarization P_x . The pulse shape is an RRC pulse with an excess bandwidth of 0.25 and a truncation length of 32 symbols.

The input bits to the DP-QPSK modulator are generated as independent, uniform random numbers. The following channel parameters are used for the numerical simulations: the nonlinear coefficients $\gamma_{SMF} = 1.4 \text{ W}^{-1}\text{km}^{-1}$, the optical frequency $\nu_{opt} = 193.55 \text{ THz}$, the attenuation coefficients $\alpha_{SMF} = 0.2 \text{ dB/km}$, $L = 125 \text{ km}$, $N = 25$, and other parameters according to Table I. Moreover, we consider two pulse shapes: An RRC [39, p. 675] with an excess bandwidth of 0.25 and a truncation length of 32 symbols and a Gaussian pulse shape with a spectral full width at half maximum (FWHM) of $2/T$ (without truncation). The CD is compensated by an EDC filter at the receiver.

In Figs. 6–7, the dashed curves represent the analytical result with DP-QPSK modulation $SER = (SER_x + SER_y)/2$, where $SER_{x(y)} = 2Q(\sqrt{\text{SNR}_{x(y)}}) - Q^2(\sqrt{\text{SNR}_{x(y)}})$ [39, eq. 4.3-15], where $\text{SNR}_{x(y)}$ is given by Theorem 1 and $Q(\cdot)$ is the Gaussian Q-function [39, p. 41]. The solid curves show the numerical results. As seen in Figs. 6–7, the model is accurate for high symbol rates ($\geq 28 \text{ Gbaud}$). As seen in Fig. 6, the SSFM SER results for a single-polarization ($\kappa = 0$) and DP ($\kappa = 1$) show a close agreement with the analytical results of the discrete-time model. However, as seen in Fig. 6, the discrete-time model loses its accuracy at SERs below 10^{-4} for System IV with a single-polarization signal, because the Gaussian approximation becomes less accurate in the tails of the distribution for finite values of η as it was shown in Fig 4. It is worth mentioning that one may exploit a parameter fitting approach to find the mapping from L_D to η . According to our observation from simulations, η decreases by increasing

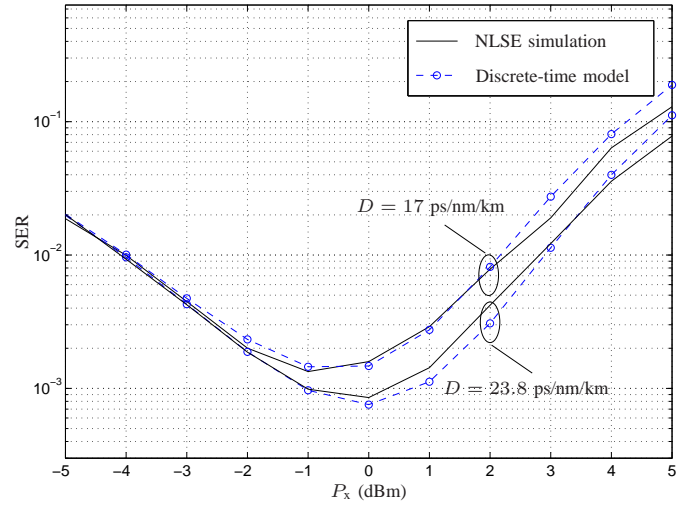


Fig. 7. The SER of systems II and III with DP-QPSK versus transmitted power per polarization P_x (D is the dispersion coefficient). A dual-polarization signal is used for both systems.

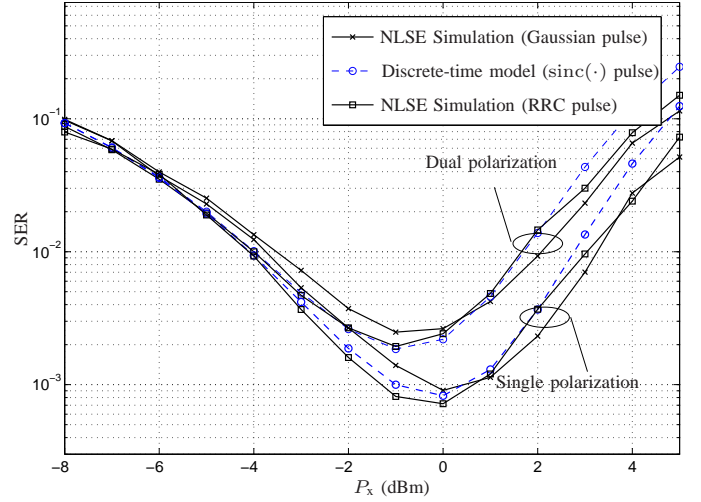


Fig. 8. The SER of system IV with single- and DP-QPSK versus transmitted power per polarization P_x for RRC and Gaussian pulse shapes.

$L_D = T^2/|\beta_2|$, as seen in Table I. Intuitively, a suitable value for η gives the best trade-off between the accuracy of SSFM and the Gaussian distribution approximation.

We also note that the system performance is improved by increasing the CD, in the nonlinear regime. As seen in Fig. 7, the system performance has been improved by increasing the dispersion coefficient from 17 to 23.8 ps/nm/km. Analytically, exploiting the results of Theorem 1, one can readily show that $\partial(\sigma_{NLx}^2)/\partial L_D \leq 0$. The impact of pulse shaping on the SER of the system is investigated in Fig. 8. As expected, its gap from the theoretical result is larger than the exploited RRC pulse.

VII. CONCLUSION

This paper introduced an analytical approach to model a nonlinear fiber-optic link as an AWGN channel for high enough symbol rates as shown in Fig. 1(b). The model was proposed for a single-channel fiber-optic link without any inline CD compensation. In this model, the channel linear response was compensated by an EDC filter at the

receiver. The attenuation and the variance of AWGN were described as a function of input power and linear and nonlinear channels parameters. The derived expression clearly revealed the interaction of a DP signal due to fiber nonlinearity. For example, the nonlinear noise in one polarization is affected twice as much by the signal power in that polarization than the orthogonal polarization. Moreover, according to the derived model, pre- and post-EDC give the same performance. The SSFM numerical results justify the accuracy of this model for a symbol rate of 28 Gbaud and above. Finally, the extension of the introduced model to a WDM case can be done by using the SSFM for a multichannel WDM link. As a future work, we expect to describe the contributions of inter-channel-interference, signal, and ASE noise interactions due to nonlinearity for a WDM scheme.

ACKNOWLEDGMENT

The authors gratefully acknowledge the anonymous reviewers for the insightful comments and constructive suggestions.

APPENDIX A THE PROOF OF LEMMA 1

We prove this lemma for the first segment with $\mathbf{V}_{1,0}[n] = \mathbf{S}[n]/\sqrt{T}$ and it is then straightforwardly extended to the other segments. To simplify the notation, we drop segment and span numbers. Here, we first show that the samples $U_x[n]$ and $U_x[n+k]$ are uncorrelated for $k \neq 0$ and $\eta \rightarrow \infty$. To this end, we need to show that their covariance and pseudo-covariance are zero [38, Lemma 1]. Then we exploit the central limit theorem under the Lyapunov condition [40, p. 362] to prove that the distribution of $U_x[n]$ converges to a Gaussian distribution for $\eta \rightarrow \infty$. Finally, we conclude that the uncorrelated Gaussian samples $U_x[n]$ are independent Gaussian samples.

Since $h[n]$ as defined in (3) is an all-pass filter, it does not affect the power spectrum of the signal, and hence $h[n] * h^\dagger[-n] = \text{sinc}(n)$. Then using (4) and the fact that the input symbols are independent and identically distributed (i.i.d.), the covariance can be expressed as

$$\begin{aligned} \text{Cov}(U_x[n+k], U_x[n] | S_x[0]) &= A^2 P_x \sum_{m \neq n+k} h[m] h^\dagger[m-k] \\ &= A^2 P_x (\text{sinc}(k) - h[n+k] h^\dagger[n]), \end{aligned} \quad (17)$$

where $\text{Cov}(X, Y) \triangleq \mathbb{E}\{XY^\dagger\} - \mathbb{E}\{X\}\mathbb{E}\{Y^\dagger\}$. Here, using Parseval's theorem, the filter coefficients $h[n]$ are computed using (3) for $\beta_2 < 0$ as

$$\begin{aligned} h[n] &= h(t, \frac{\eta}{2} L_D) * \text{sinc}\left(\frac{t}{T}\right) \Big|_{t=nT} = \int_{-\infty}^{+\infty} \frac{e^{\frac{j}{\eta}(n-\tau)^2}}{\sqrt{j\pi\eta}} \text{sinc}(\tau) d\tau \\ &= \frac{1}{\pi\sqrt{\eta}} e^{\frac{j}{\eta}n^2} \int_{a_n^-}^{a_n^+} e^{-jf^2} df, \end{aligned} \quad (18)$$

where $\sqrt{\eta}a_n^\pm = n \pm \eta\pi/2$. For $\eta \gg 1$, using [41, eq. 8.255] and (18), one can show that

$$|h[n]| < \begin{cases} \frac{8}{\pi\sqrt{\eta}}, & |n| \leq \eta\pi, \\ \frac{C_1}{\sqrt{\eta}|a_n^-|}, & \text{elsewhere,} \end{cases} \quad (19)$$

where C_1 is a constant factor. Substituting (19) into (17), we obtain $\lim_{\eta \rightarrow \infty} \text{Cov}(U_x[n+k], U_x[n] | S_x[0]) = 0$, for $k \neq 0$. Now, we need to show that their pseudo-covariance is also zero, and this follows directly from $\text{Cov}(U_x[n+k], U_x^\dagger[n] | S_x[0]) = A^2 \sum_{m \neq n+k} \mathbb{E}\{S_x^2[n+k-m] | S_x[0]\} h[m] h[m-k]/T$. Since the input symbols are a sequence of proper complex random variables, $\mathbb{E}\{S_x^2[p] | S_x[0]\} = 0$ for $p \neq 0$, and consequently the pseudo-covariance is zero.

Next, we show that the distribution of the samples given in (4) for the first segment converges to a Gaussian distribution when $\eta \rightarrow \infty$. For this purpose, we can apply the central limit theorem [40, p. 362] for the sum of non-identical variables $h[k]S_x[k]$ in (4) under the Lyapunov condition. The Lyapunov condition [40, p. 362]

$$\lim_{K \rightarrow \infty} \frac{\sum_{k=-K}^K \mathbb{E}\{|h[k]S_x[k]|^{2+\delta}\}}{\left(\sum_{k=-K}^K \mathbb{E}\{|h[k]S_x[k]|^2}\right)^{1+\frac{\delta}{2}}} = 0, \quad (20)$$

needs to be fulfilled for some positive δ for the central limit theorem to be applicable to the independent non-identical random variables $h[k]S_x[k]$. The denominator of (20) can be written by using the i.i.d. property of the input symbols and Parseval's theorem as $[(1 - |h[0]|^2)P_x T]^{1+\frac{\delta}{2}}$, which is independent of K and η . The numerator of (20) can also be simplified as $C_2 \lim_{K \rightarrow \infty} \sum_{k=-K, k \neq 0}^K |h[k]|^{2+\delta}$, where $C_2 = \mathbb{E}_{k \neq 0}\{|S_x[k]|^{2+\delta}\}$ is independent of K and η . Thus, we can proceed with the Lyapunov condition by exploiting (19) as

$$\begin{aligned} \lim_{K \rightarrow \infty} \sum_{k=-K, k \neq 0}^K |h[k]|^{2+\delta} &= \sum_{k=-\eta\pi, k \neq 0}^{\eta\pi} |h[k]|^{2+\delta} + \lim_{K \rightarrow \infty} 2 \sum_{k=\eta\pi}^K |h[k]|^{2+\delta} \\ &< C_3 \eta^{-\frac{\delta}{2}} + 2C_1^{2+\delta} \lim_{K \rightarrow \infty} \sum_{k=\frac{\eta}{2}\pi}^K k^{-2-\delta}, \end{aligned}$$

where $C_3 = 2^{7+3\delta}/\pi^{1+\delta}$. Since $k^{-2-\delta}$ is a positive decreasing function for $k > \eta\pi/2$,

$$\begin{aligned} \lim_{K \rightarrow \infty} \sum_{k=-K, k \neq 0}^K |h[k]|^{2+\delta} &< C_3 \eta^{-\frac{\delta}{2}} + 2C_1^{2+\delta} \lim_{K \rightarrow \infty} \int_{x=\frac{\eta\pi}{2}-1}^K x^{-2-\delta} dx \\ &< C_3 \eta^{-\frac{\delta}{2}} + 2 \frac{C_1^{2+\delta}}{2+\delta-1} \left(\frac{\eta\pi}{2} - 1\right)^{-2-\delta+1}. \end{aligned}$$

The right side of this inequality converges to zero for $\eta \rightarrow \infty$. Thus, the Lyapunov condition is fulfilled. Finally, it can be readily concluded that the uncorrelated Gaussian samples are independent, which completes the proof for the first segment. Considering the memory-less nonlinear operation in Stage 2 of Fig. 3(a) and applying an analogous approach, it can be readily shown that the samples $V[n]$ are i.i.d. for $\eta \rightarrow \infty$. Therefore, one can conclude that the same proof is valid for also the other segments ($m > 1$).

APPENDIX B PROPOSITION 1

Proposition 1: If X is a proper complex Gaussian random variable with mean \bar{X} and variance σ_X^2 , ξ is a constant real coefficient, and n is an integer, then

$$\mathbb{E} \left\{ |X|^2 e^{j\xi|X|^2} \right\} = (|\bar{X}|^2 + \sigma_X^2 - j\xi\sigma_X^4) (1 - j\xi\sigma_X^2)^{-3} e^{j\frac{\xi|\bar{X}|^2}{1-j\xi\sigma_X^2}}, \quad (21)$$

$$\mathbb{E} \left\{ X^n e^{j\xi|X|^2} \right\} = \bar{X}^n (1 - j\xi\sigma_X^2)^{-(n+1)} e^{j\frac{\xi|\bar{X}|^2}{1-j\xi\sigma_X^2}}, \quad 0 \leq n \leq 2. \quad (22)$$

Proof: Let $X = X_r + jX_i$, where X_r and X_i are real, Gaussian random variables with mean μ_r and μ_i , resp., and the same variance $\sigma_X^2/2$. Then $\mathbb{E}\{|X|^2 e^{j\xi|X|^2}\} = a_2 b_0 + a_0 b_2$, $\mathbb{E}\{e^{j\xi|X|^2}\} = a_0 b_0$, $\mathbb{E}\{X e^{j\xi|X|^2}\} = a_1 b_0 + j a_0 b_1$, and $\mathbb{E}\{X^2 e^{j\xi|X|^2}\} = a_2 b_0 + 2j a_1 b_1 - a_0 b_2$, where $a_n = \mathbb{E}\{X_r^n e^{j\xi X_r^2}\}$ and $b_n = \mathbb{E}\{X_i^n e^{j\xi X_i^2}\}$. The lemma follows by expressing a_n and b_n for $n = 0, 1, 2$ as one-dimensional integrals, calculating these integrals exactly using [41, eqs. 3.323.2, 3.462.6, 3.462.8], substituting $\mu_r + j\mu_i = \bar{X}$, and simplifying. ■

APPENDIX C PROOF OF LEMMA 2

By an analogous approach as in the proof of Lemma 1, we begin with the proof for the first segment and it is then straightforwardly extended to the other segments. To simplify the notation, we also drop segment and span numbers. First, we show that $|\bar{U}_x[n]|^2$ and $|\bar{U}_x[n]\bar{U}_y^\dagger[n]|$ tend to zero as $\eta \rightarrow \infty$. To this end, for a given transmitted symbol vector $\mathbf{s} = (s_x, s_y)$, one may use (4), (17), and the model introduced in Figs. 2 and 3(a) to get $|\bar{U}_x[n]|^2 = |s_x|^2 |h[n]|^2 / T$ and $|\bar{U}_y[n]|^2 = |s_y|^2 |h[n]|^2 / T$. Now, using (19), it is clearly seen that

$$\lim_{\eta \rightarrow \infty} |\bar{U}_x[n]|^2 = 0, \quad \lim_{\eta \rightarrow \infty} |\bar{U}_x[n]\bar{U}_y^\dagger[n]| = 0. \quad (23)$$

A. The nonlinear noise $V_{NL_x}[n]$ and $V_{NL_y}[n]$ are independent

We first show that $V_{NL_x}[n]$ and $V_{NL_y}[n]$ are proper Gaussian random variables. Then, we solely need to show that both their covariance and pseudo-covariance are zero [38, Lemma 1]. Since a complex proper random variable after a linear or affine transformation stays proper [38, Lemma 3], one can conclude using Lemma 1 that $U_x[n]$ is a sequence of independent complex proper Gaussian random variables. Moreover, it is clearly seen from (7) that $\mathbf{B}[n]$ is also a sequence of independent random variables. Therefore, one can exploit an analogous approach as in the proof of Lemma 1 to conclude that $V_{NL_x}[n]$ and $V_{NL_y}[n]$ are sequences of independent Gaussian random variables. Here, we show that $V_{NL_x}[n]$ and $V_{NL_y}[n]$ are also proper. Hence, we need to show that $\mathbb{E}\{V_{NL_x}[n]V_{NL_x}^\dagger[n]|S_x[0]\} = 0$ [38, Definition 1]. Using (7), we get

$$\mathbb{E} \left\{ V_{NL_x}[n]V_{NL_x}^\dagger[n]|S_x[0] \right\} = A^2 \sum_{m,p} \mathbb{E} \left\{ B_x[n-m]B_x[n-p]|S_x[0] \right\} \times h[m]h[p] = A^2 \mathbb{E} \left\{ B_x^2[n]|S_x[0] \right\} * h^2[n]. \quad (24)$$

Since U_x is a proper Gaussian random process, $\mathbb{E}\{U_x^2[n]|S_x[0]\} = \bar{U}_x^2$. Then, using Proposition 1, we obtain

$$\mathbb{E} \left\{ B_x^2[n]|S_x[0] \right\} = \mathbb{E} \left\{ U_x^2[n] e^{2j\mu \| \mathbf{U}[n] \|^2} |S_x[0] \right\} - 2\zeta_x[n] \times \mathbb{E} \left\{ U_x^2[n] e^{j\mu \| \mathbf{U}[n] \|^2} |S_x[0] \right\} + \zeta_x^2[n] \mathbb{E} \left\{ U_x^2[n]|S_x[0] \right\} \quad (25)$$

$$= \bar{U}_x[n]^2 \left[\zeta_x^2[n] + (1 - 2j\mu\sigma_{\bar{U}_x}^2)^{-3} (1 - 2j\mu\sigma_{\bar{U}_y}^2)^{-1} \right. \\ \left. \times e^{2j\mu \left(\frac{|\bar{U}_x[n]|^2}{1 - 2j\mu\sigma_{\bar{U}_x}^2} + \frac{|\bar{U}_y[n]|^2}{1 - 2j\mu\sigma_{\bar{U}_y}^2} \right)} - 2\zeta_x[n]\Phi_x^3[n]\Phi_y[n] \right. \\ \left. \times e^{j\mu(\Phi_x[n]|\bar{U}_x[n]|^2 + \Phi_y[n]|\bar{U}_y[n]|^2)} \right].$$

By substituting (25) into (24) and using (23), one can readily show that the pseudo-covariance of $V_{NL_x}[n]$ is zero, i.e., $\lim_{\eta \rightarrow \infty} |\text{Cov}(V_{NL_x}[n], V_{NL_x}^\dagger[n]|S_x[0])| = 0$. Thus, $V_{NL_x}[n]$ is a sequence of proper Gaussian random variables. Until now, we have shown that the complex random sequence $V_{NL_x}[n]$ and similarly $V_{NL_y}[n]$ are sequences of proper Gaussian random variables. Therefore, to prove that they are uncorrelated, we need to show that both their covariance and pseudo-covariance are zero [38, Lemma 1]. Exploiting (7) and Proposition 1, we obtain

$$\mathbb{E} \left\{ V_{NL_x}[n]V_{NL_y}^\dagger[n]|S[0] \right\} = A^2 \sum_{m,p} \mathbb{E} \left\{ B_x[n-m]B_y^\dagger[n-p]|S[0] \right\} \\ \times h[m]h^\dagger[p] = A^2 \mathbb{E} \left\{ B_x[n]B_y^\dagger[n]|S[0] \right\} * |h[n]|^2, \\ \mathbb{E} \left\{ B_x[n]B_y^\dagger[n]|S[0] \right\} = \bar{U}_x[n]\bar{U}_y^\dagger[n] \left(1 + \zeta_x[n]\zeta_y[n] - \zeta_x[n] \right. \\ \left. \times (\Phi_x^2[n]\Phi_y^2[n])^\dagger e^{-j\mu(\Phi_x^\dagger[n]|\bar{U}_x[n]|^2 + \Phi_y^\dagger[n]|\bar{U}_y[n]|^2)} \zeta_y^\dagger[n]\Phi_x^2[n]\Phi_y^2[n] \right. \\ \left. \times e^{j\mu(\Phi_x[n]|\bar{U}_x[n]|^2 + \Phi_y[n]|\bar{U}_y[n]|^2)} \right). \quad (26)$$

Proceeding similarly,

$$\mathbb{E} \left\{ V_{NL_x}[n]V_{NL_y}[n]|S[0] \right\} = A^2 \sum_{m,p} \mathbb{E} \left\{ B_x[n-m]B_y[n-p]|S[0] \right\} \\ \times h[m]h[p] = A^2 \mathbb{E} \left\{ B_x[n]B_y[n]|S[0] \right\} * h^2[n], \\ \mathbb{E} \left\{ B_x[n]B_y[n]|S[0] \right\} = \bar{U}_x[n]\bar{U}_y[n] \left[\zeta_x[n]\zeta_y[n] - (\zeta_x[n] + \zeta_y[n]) \right. \\ \left. \times \Phi_x^2[n]\Phi_y^2[n] e^{j\mu(\Phi_x[n]|\bar{U}_x[n]|^2 + \Phi_y[n]|\bar{U}_y[n]|^2)} + (1 - 2j\mu\sigma_{\bar{U}_x}^2)^{-2} \right. \\ \left. \times (1 - 2j\mu\sigma_{\bar{U}_y}^2)^{-2} \exp \left(\frac{2j\mu|\bar{U}_x[n]|^2}{1 - 2j\mu\sigma_{\bar{U}_x}^2} + \frac{2j\mu|\bar{U}_y[n]|^2}{1 - 2j\mu\sigma_{\bar{U}_y}^2} \right) \right].$$

Here, using (23), we obtain $\lim_{\eta \rightarrow \infty} |\text{Cov}(V_{NL_x}[n], V_{NL_x}^\dagger[n]|S[0])| = 0$ and $\lim_{\eta \rightarrow \infty} |\text{Cov}(V_{NL_x}[n], V_{NL_x}[n]|S[0])| = 0$. Therefore, $V_{NL_x}[n]$ and $V_{NL_y}[n]$ are independent.

B. The received signal, $V_L[n]$, and the nonlinear noise, $V_{NL_x}[n]$, are independent

According to Lemma 1, $V_L[n]$ and $V_{NL_x}[n]$ are proper Gaussian random variables. Therefore, we solely need to show that for $\eta \rightarrow \infty$, their covariance and pseudo-covariance are both zero. Using (7) and Proposition 1, this follows as

$$\mathbb{E} \left\{ V_{NL_x}[n]V_L^\dagger[n]|S_x[0] \right\} = A^2 \zeta_x^\dagger[n] \sum_{m,p} \mathbb{E} \left\{ B_x[n-m]U_x^\dagger[n-p] \right. \\ \left. |S_x[0] \right\} h[m]h^\dagger[p] = A^2 \zeta_x^\dagger[n] \mathbb{E} \left\{ B_x[n]U_x^\dagger[n]|S_x[0] \right\} * |h[n]|^2,$$

$$\mathbb{E} \left\{ B_x[n]U_x^\dagger[n]|S_x[0] \right\} = \zeta_x^\dagger[n] \left(\mathbb{E} \left\{ |U_x[n]|^2 e^{j\mu \| \mathbf{U}[n] \|^2} |S_x[0] \right\} \right. \\ \left. - \zeta_x[n] \mathbb{E} \left\{ |U_x[n]|^2 |S_x[0] \right\} \right) = |\bar{U}_x[n]|^2 (\zeta_x^\dagger[n]\Phi_x[n] - \zeta_x^\dagger[n]).$$

Proceeding similarly, we get

$$\begin{aligned}\mathbb{E}\{V_{\text{NL}_x}[n]V_{\text{L}_x}[n]|S_x[0]\} &= A^2\zeta_x^\dagger[n]\mathbb{E}\{B_x[n]U_x[n]|S_x[0]\} * |h[n]|^2 \\ &= A^2\bar{U}_x[n]^2(\zeta_x[n]\Phi_x[n] - \zeta_x[n]).\end{aligned}$$

Thus, using (23), we obtain $\lim_{\eta \rightarrow \infty} |\text{Cov}(V_{\text{NL}_x}[n], V_{\text{L}_x}[n]|S_x[0])| = 0$ and $\lim_{\eta \rightarrow \infty} |\text{Cov}(V_{\text{NL}_x}[n], V_{\text{L}_x}^\dagger[n]|S_x[0])| = 0$. This concludes that $V_{\text{NL}_x}[n]$ and $V_{\text{L}_x}[n]$ and similarly $V_{\text{NL}_y}[n]$ and $V_{\text{L}_y}[n]$ are independent. Since by induction, it can be shown that (23) is valid for all segments, the same proof holds for also the other segments ($m > 1$).

APPENDIX D

THE CHANNEL ATTENUATION AND THE NONLINEAR NOISE VARIANCE OF A SEGMENT

In this appendix, the derivation of the approximation given in Section IV-B1 is described. We first show that (23) is also approximately valid for a system in the linear regime with a finite η . Then, we use it as an approximation in the pseudo-linear regime [6] to derive the squared amplitude of the channel attenuation and the nonlinear noise variance of a segment. For a given transmitted symbol $S_x[0] = s_x$, the mean of the input of the first segment is $\mathbb{E}\{V_{x_0^1}[n]|S_x[0]\} = s_x/\sqrt{T}$ at $n = 0$ and 0 for $n \neq 0$. Moreover, $\text{Var}(V_{x_0^1}[n]|S_x[0]) = 0$ at $n = 0$ and P_x for $n \neq 0$. Furthermore, if we assume that $h_z[n]$ is the channel response for a fiber length of z in the linear regime, $U_{x_m^i}[n] = A^{2m-1} \sum_{k=-\infty}^{\infty} V_{x_0^1}[n-k]h_{\ell_{i,m}}[k]$, where $\ell_{i,m} = (2m-1)\eta L_D/2 + (i-1)L$ is the fiber length from the beginning of the link to the midpoint of segment m in span i . The squared magnitude of the CD filter coefficients, for a fiber length of z , can be approximated [34, eq. 9] by

$$|h_z[n]|^2 \approx \begin{cases} \frac{L_D}{2\pi z}, & |n| \leq \frac{\pi z}{L_D}, \\ 0, & \text{elsewhere.} \end{cases} \quad (27)$$

Thus, for $|n| \leq \pi\ell_{i,m}/L_D$,

$$|\bar{U}_{x_m^i}[n]|^2 = \frac{1}{T}|h_{\ell_{i,m}}[n]|^2|s_x|^2 A^{4m-2} \approx \frac{1}{\ell_{i,m}T}|s_x|^2 A^{4m-2} L_D$$

and

$$\begin{aligned}\text{Var}(U_{x_m^i}[n]) &= A^{4m-2} P_x \sum_{k \neq n} |h_{\ell_{i,m}}[k]|^2 + (i-1)\sigma^2 A^{4m-2} \\ &= A^{4m-2} P_x (1 - |h_{\ell_{i,m}}[n]|^2) + (i-1)\sigma^2 A^{4m-2} \\ &\approx A^{4m-2} P_x \left(1 - \frac{L_D}{2\pi\ell_{i,m}}\right) + (i-1)\sigma^2 A^{4m-2},\end{aligned}$$

where we used $\sum_{k=-\infty}^{\infty} |h_{\ell_{i,m}}[k]|^2 = 1$ because $h_{\ell_{i,m}}[k]$ is an all-pass filter with unity gain. Here, we note that for $m \geq 4$, $L_D/2\pi\ell_{i,m} \approx 0$ and hence

$$\frac{|\bar{U}_{x_m^i}[n]|^2}{P_x} \approx 0, \quad (28)$$

$$\text{Var}(U_{x_m^i}[n]) \approx (P_x + (i-1)\sigma^2) A^{4m-2}. \quad (29)$$

For the sake of simplicity, we apply this approximation for all segments including $m \leq 4$. Although the approximation for the first four segments is not accurate, the numerical results (see section VI) justify that for a large enough number of spans ($N > 10$), its effect is negligible.

Now, for a given transmitted symbols $\mathbf{s}[0] = (s_x, s_y)$, one may substitute (28) into (8) to get

$$|\Phi_{x_m^i}|^{-2} \approx 1 + 4\phi_x^2 \left[1 + (i-1)\frac{1}{N\rho_x}\right]^2 \sinh^2\left(\frac{\alpha}{2}\eta L_D\right) A^{8m-4}, \quad (30)$$

$$|\Phi_{y_m^i}|^{-2} \approx 1 + 4\phi_x^2 \left[\kappa + (i-1)\frac{1}{N\rho_x}\right]^2 \sinh^2\left(\frac{\alpha}{2}\eta L_D\right) A^{8m-4}, \quad (31)$$

where $\kappa = P_y/P_x$. Finally, by substituting (28), (30), and (31) into (9), then doing a Taylor expansion with respect to ϕ_x , and neglecting the terms of order higher than ϕ_x^2 , we get (11).

According to (5), the signal at the output of each segment can be decomposed into a linear, $V_{\text{L}_m^i}[n]$, and a nonlinear, $V_{\text{NL}_m^i}[n]$, term. In addition, using Lemma 2, the linear and nonlinear terms are independent. Therefore, $\text{Var}\{V_{x_m^i}[n]\} = \text{Var}\{V_{\text{L}_m^i}[n]\} + \text{Var}\{V_{\text{NL}_m^i}[n]\}$. Here, we exclude the ASE noises from linear and nonlinear terms and the accumulated ASE noise is considered with the variance of $(i-1)\sigma^2 A^{4m}$ at the output the segment. Since the channel is nonlinear, the signal and the ASE noise are not treated independently and we solely decompose them to describe the received signal as a sum of three components: the signal without noise and nonlinear interference, the nonlinear noise, and the ASE noise. Now, using (6) and (28), it is seen that the signal power (excluding the ASE noise and the nonlinear interference) is $|\zeta_{x_m^i}|^2 A^{4m} P_x$ and the variance of the nonlinear noise is $(1 - |\zeta_{x_m^i}|^2) A^{4m} P_x$ for polarization x , as given in (12).

APPENDIX E

PROOF OF THEOREM 1

First, we derive the channel model for span i , where $1 \leq i \leq N$, of an optical-fiber link. Then, we extend the results to a link with N spans.

Lemma 3: Assuming equalities in (11) and (12), span i of a fiber-optical link can be modeled by an AWGN channel as shown in Fig. 1(b). The squared magnitude of the channel complex scaling in polarization x is given by

$$\begin{aligned}|\zeta_x^i|^2 &= 1 - \tanh\left(\frac{\alpha}{2}\eta L_D\right) (1 - e^{-2\alpha L}) \left[2 + \kappa^2 + 2(i-1)\frac{2+\kappa}{N\rho_x}\right. \\ &\quad \left. + (i-1)^2 \frac{3}{N^2\rho_x^2}\right] \phi_x^2.\end{aligned} \quad (32)$$

The accumulated nonlinear noise variance in polarization x is $\sigma_{\text{NL}_x^i}^2 = P_x(1 - |\zeta_x^i|^2)$.

Proof: As shown in Fig. 3(a), span i can be modeled as M serially concatenated segments. Substituting (11) into the total complex scaling given by $\zeta_x^i = \prod_{m=1}^M \zeta_{x_m^i}$ and performing some algebraic manipulations, one can easily get (32). The variance of the nonlinear noise accumulated from M segments of span i at the end of this span is $\sigma_{\text{NL}_x^i}^2 = P_x(1 - \prod_{k=1}^M |\zeta_{x_k^i}|^2) = P_x(1 - |\zeta_x^i|^2)$. ■

We now extend the results to a fiber link with N spans by following an analogous approach. One may view the channel given in Fig. 2 as a concatenation of N channels described by Lemma 3. The linear noise, which is independent from the added nonlinear noise, is added with variance σ^2 at the end of each span. Since multiplication by a constant commutes with convolution, the channel attenuation in different spans can be

moved to the end of the last span. Thus, by following the same approach as the proof of Lemma 3, one can readily derive the squared magnitude of the total complex scaling by substituting ζ_{x^i} into $\zeta_x = \prod_{i=1}^N \zeta_{x^i}$.

As we discussed in Appendix D, the variance of the accumulated AWGN at the receiver is the sum of the variances of the amplifier noises added along the fiber-optic link, i.e., $N\sigma^2$. Moreover, the signal power P_x is split into a linear part with variance $|\zeta_x|^2 P_x$ and a nonlinear part with variance $\sigma_{NL}^2 = (1 - |\zeta_x|^2) P_x$. The nonlinear part acts as an noise-like interference and is called nonlinear noise. Finally, the system SNR can be computed as the ratio of the received signal power to the sum of the linear and nonlinear noise variances.

REFERENCES

- [1] P. J. Winzer and R.-J. Essiambre, "Advanced modulation formats for high-capacity optical transport networks," *J. Lightwave Technol.*, vol. 24, no. 12, pp. 4711–4728, Dec. 2006.
- [2] E. Agrell and M. Karlsson, "Power-efficient modulation formats in coherent transmission systems," *J. Lightwave Technol.*, vol. 27, no. 22, pp. 5115–5126, Nov. 2009.
- [3] G. D. Forney, Jr. and G. Ungerboeck, "Modulation and coding for linear Gaussian channels," *IEEE Trans. Inform. Theory*, vol. 44, no. 6, pp. 2384–2415, Oct. 1998.
- [4] E. Ip, A. P. T. Lau, D. J. F. Barros, and J. M. Kahn, "Coherent detection in optical fiber systems," *Opt. Express*, vol. 16, no. 2, pp. 753–791, 2008.
- [5] G. D. Forney, Jr. and D. J. Costello, Jr., "Channel coding: The road to channel capacity," *Proc. IEEE*, vol. 95, no. 6, pp. 1150–1177, Jun. 2007.
- [6] R. J. Essiambre, G. Kramer, P. J. Winzer, G. J. Foschini, and B. Goebel, "Capacity limits of optical fiber networks," *J. Lightwave Technol.*, vol. 28, no. 4, pp. 662–701, Feb. 2010.
- [7] A. D. Ellis, J. Zhao, and D. Cotter, "Approaching the non-linear Shannon limit," *J. Lightwave Technol.*, vol. 28, no. 4, pp. 423–433, Feb. 2010.
- [8] A. Mecozzi, "Probability density functions of the nonlinear phase noise," *Opt. Lett.*, vol. 29, no. 7, pp. 673–675, 2004.
- [9] K.-P. Ho, *Phase-Modulated Optical Communication Systems*. Springer, New York, 2005.
- [10] L. Beygi, E. Agrell, M. Karlsson, and P. Johannisson, "Signal statistics in fiber-optical channels with polarization multiplexing and self-phase modulation," *J. Lightwave Technol.*, vol. 29, no. 16, pp. 2379–2386, Aug. 2011.
- [11] A. P. T. Lau, T. S. R. Shen, W. Shieh, and K.-P. Ho, "Equalization-enhanced phase noise for 100Gb/s transmission and beyond with coherent detection," *Opt. Express*, vol. 18, no. 16, pp. 17239–17251, Aug. 2010.
- [12] K.-P. Ho, A. P. T. Lau, and W. Shieh, "Equalization-enhanced phase noise induced timing jitter," *Opt. Lett.*, vol. 36, no. 4, pp. 585–587, Feb. 2011.
- [13] B. Goebel, R.-J. Essiambre, G. Kramer, P. J. Winzer, and N. Hanik, "Calculation of mutual information for partially coherent Gaussian channels with applications to fiber optics," *IEEE Trans. Inform. Theory*, vol. 57, no. 9, pp. 5720–5736, Sep. 2011.
- [14] A. T. Lau, S. Rabbani, and J. M. Kahn, "On the statistics of intrachannel four-wave mixing in phase-modulated optical communication systems," *J. Lightwave Technol.*, vol. 26, no. 14, pp. 2128–2135, Jul. 2008.
- [15] K.-P. Ho and H.-C. Wang, "Comparison of nonlinear phase noise and intrachannel four-wave mixing for RZ-DPSK signals in dispersive transmission systems," *IEEE Photon. Technol. Lett.*, vol. 17, no. 7, pp. 1426–1428, Jul. 2005.
- [16] J. P. Gordon and L. F. Mollenauer, "Phase noise in photonic communications systems using linear amplifiers," *Opt. Lett.*, vol. 15, no. 23, pp. 1351–1353, 1990.
- [17] S. Kumar, "Effect of dispersion on nonlinear phase noise in optical transmission systems," *Opt. Lett.*, vol. 30, no. 24, pp. 3278–3280, Dec. 2005.
- [18] K.-P. Ho and H.-C. Wang, "Effect of dispersion on nonlinear phase noise," *Opt. Lett.*, vol. 31, no. 14, pp. 2109–2111, Jul. 2006.
- [19] M. Secondini, E. Forestieri, and C. R. Menyuk, "A combined regular-logarithmic perturbation method for signal-noise interaction in amplified optical systems," *J. Lightwave Technol.*, vol. 27, no. 16, pp. 3358–3369, Aug. 2009.
- [20] M. Secondini, M. Frezzini, and E. Forestieri, "Analytical performance evaluation of optical DQPSK systems with postdetection filtering," *IEEE Photon. Technol. Lett.*, vol. 21, pp. 908–910, 2009.
- [21] E. Forestieri and M. Secondini, "On the error probability evaluation in lightwave systems with optical amplification," *J. Lightwave Technol.*, vol. 27, no. 6, pp. 706–717, Mar. 2009.
- [22] H. Song and M. Brandt-Pearce, "A discrete-time polynomial model of single channel long-haul fiber-optic communication systems," in *Proc. of IEEE Int. Conf. on Commun.*, Jun. 2011, Kyoto, Japan.
- [23] A. Carena, G. Bosco, V. Curri, P. Poggiolini, M. Taiba, and F. Forghieri, "Statistical characterization of PM-QPSK signals after propagation in uncompensated fiber links," in *Proc. of European Conf. and Exhibition on Optic. Commun.*, Sep. 2010, P4.07.
- [24] G. Bosco, A. Carena, R. Cigliutti, V. Curri, P. Poggiolini, and F. Forghieri, "Performance prediction for WDM PM-QPSK transmission over uncompensated links," in *Proc. of Optic. Fiber Commun. Conf.*, 2011, OThO7.
- [25] P. Poggiolini, A. Carena, V. Curri, G. Bosco, and F. Forghieri, "Analytical modeling of nonlinear propagation in uncompensated optical transmission links," *IEEE Photon. Technol. Lett.*, vol. 23, no. 11, pp. 742–744, Jun. 2011.
- [26] A. Carena, V. Curri, G. Bosco, P. Poggiolini, and F. Forghieri, "Modeling of the impact of Non-Linear propagation effects in uncompensated optical coherent transmission links," *J. Lightwave Technol.*, 2012, to appear.
- [27] A. Bononi, E. Grellier, P. Serena, N. Rossi, and F. Vacondio, "Modeling nonlinearity in coherent transmissions with dominant interpulse-four-wave-mixing," in *Proc. of European Conf. and Exhibition on Optic. Commun.*, 2011, We.7.B.4.
- [28] E. Grellier and A. Bononi, "Quality parameter for coherent transmissions with Gaussian-distributed nonlinear noise," *Opt. Express*, vol. 19, no. 13, pp. 12781–12788, Jun. 2011.
- [29] A. Mecozzi and F. Matera, "Intrachannel nonlinearity enhancement in polarization multiplexed phase modulated systems with differential detection," *Opt. Lett.*, vol. 36, no. 19, pp. 3903–3905, Oct. 2011.
- [30] —, "Polarization scattering by intra-channel collisions," *Opt. Express*, vol. 20, no. 2, pp. 1213–1218, Jan. 2012.
- [31] G. P. Agrawal, *Nonlinear fiber optics*, 4th ed. Academic Press, 2007.
- [32] D. Wang and C. Menyuk, "Polarization evolution due to the Kerr nonlinearity and chromatic dispersion," *J. Lightwave Technol.*, vol. 17, no. 12, pp. 2520–2529, Dec. 1999.
- [33] R. Killely, P. Watts, V. Mikhailov, M. Glick, and P. Bayvel, "Electronic dispersion compensation by signal predistortion using digital processing and a dual-drive Mach-Zehnder modulator," *IEEE Photon. Technol. Lett.*, vol. 17, no. 3, pp. 714–716, Mar. 2005.
- [34] S. J. Savory, "Digital filters for coherent optical receivers," *Opt. Express*, vol. 16, no. 2, pp. 804–817, Jan. 2008.
- [35] G. P. Agrawal, *Fiber-Optic Communication Systems*, 2nd ed. Wiley, 2002.
- [36] E. Ip and J. M. Kahn, "Compensation of dispersion and nonlinear impairments using digital backpropagation," *J. Lightwave Technol.*, vol. 26, no. 20, pp. 3416–3425, Oct. 2008.
- [37] A. Mecozzi, C. Clausen, and M. Shtaif, "Analysis of intrachannel nonlinear effects in highly dispersed optical pulse transmission," *IEEE Photon. Technol. Lett.*, vol. 12, no. 4, pp. 392–394, Apr. 2000.
- [38] F. Neeser and J. Massey, "Proper complex random processes with applications to information theory," *IEEE Trans. Inform. Theory*, vol. 39, no. 4, pp. 1293–1302, Jul. 1993.
- [39] J. G. Proakis and M. Salehi, *Digital Communications*, 5th ed. McGraw-Hill, 2008.
- [40] P. Billingsley, *Probability and Measure*, 3rd ed. Wiley, 1995.
- [41] I. S. Gradshteyn and I. M. Ryzhik, *Table of Integrals, Series, and Products*, 5th ed. Academic Press, 1994.